Orthogonal Multitone Electrical Impedance Spectroscopy - OMEIS - for the Study of Fibrosis Induced by Active Cardiac Implants

Edwin de Roux, Amélie Degache, Mehdi Terosiet, Florian Kolbl, Michel
Boissière, Emmanuel Pauthe, Aymeric Histace, Olivier Bernus, Noëlle Lewis,
Olivier Romain

HAL Id: hal-02078281

https://hal.science/hal-02078281

Submitted on 25 Mar 2019

Orthogonal Multitone Electrical Impedance Spectroscopy - OMEIS - for the Study of Fibrosis Induced by Active Cardiac Implants

Edwin De Roux[1,5], Amelie Degache[3], Mehdi Terosiet[1], Florian Kölbl[1], Michel Boissière[2], Emmanuel Pauthe[2], Aymeric Histace[1], Olivier Bernus[4], Noëlle Lewis[3], Olivier Romain[1]

[1]*Laboratoire ETIS, Université Paris Seine, Université de Cergy-Pontoise, ENSEA, CNRS, UMR8051*
[2]*Laboratoire ERRMECe, Université Paris Seine, Université de Cergy-Pontoise, EA1391*
[3]*IMS Bordeaux, Université Bordeaux, UMR5218*
[4]*IHU LIRYC, Univ. Bordeaux, Inserm CRCTB U1045, F-33600, Pessac, France*
[5]*SENACYT and Universidad Tecnológica de Panamá. edwin.de-roux@ensea.fr*

Correspondence should be addressed to Edwin De Roux; edwin.de-roux@ensea.fr

Fibrosis represents an open issue for mid to long-term active implants, like pacemakers, given that this biological tissue surrounds the stimulation electrodes and can impact or modify the performances of the system. For this reason, we present a strategy for the continuous sensing of fibrosis induced by cardiac implants, based on the use of the same set of electrodes involved in the implant stimulation process and whose implementation can be integrated into the pacing and sensing circuitry of pacemakers. To do this, the proposed measurement system complies with certain requirements for its integration, such as rapid measurement time, flexibility, low power consumption and low use of resources. This was achieved through the use of an orthogonal multitone stimulation signal and the design of an Orthogonal Frequency Division Multiplexing (OFDM) architecture that are the bases of the system. As a proof of concept, we implemented this technique within a FPGA. Initial tests of this system have been performed through *in vitro* measurements of cell cultures related to fibrosis, which, once validated, have allowed us to advance to *ex vivo* measurements of inhibited and perfused cardiac tissue; conditions that offer a first view for *in vivo* measurements. This article describes the measurement system implemented and also discusses the results of its validation and of the *in vitro* and *ex vivo* measurements, comparing them with results obtained by a reference instrument.

1. Introduction

Over the last fifty years, electrotherapy has shown a very rapid development with many innovators contributing to a whole series of devices. Electrotherapy uses an external source of electricity to stimulate human tissue in ways that produce a beneficial therapeutic effect. The best known electrotherapy devices are the active implantable medical devices, among them cardiac defibrillators (1949), Peacemakers (PCM) (1957), cochlear (1971) and deep brain (2000) stimulators.

These systems use the latest micro-nano-electronics technologies, with electrodes that stimulate and sense the surrounding biological environment. Such implanted devices induce an immediate and sustained inflammatory response of the body. This chronic and unresolved inflammation induces fibrosis, which is a complex biological process involving multiscale phenomena. At the cellular scale, fibroblasts are activated and differentiate to myofibroblasts; at the tissular scale, excessive secretion of extracellular matrix components, like collagen, finally produces a dense fibrous capsule around the implants, especially the electrodes [1].

In case of PCM, fibrosis reduces both the functionality and the efficacy of the implant to target the desired tissue, diverting even the stimulating current to unforeseen regions and altering the impedance of the tissue around electrodes. Furthermore, it could change the shape and magnitude of the electric field generated [2] and forces the increase of the PCM stimulation threshold and the reduction of battery lifespan [3].

The fibrosis can be treated medically to reduce its consequences, but the effectiveness of the treatment depends on the accurate diagnosis. The standard method for determining the degree of tissue reaction surrounding implanted electrodes is histology. Immunohistochemical methods enable the visualization of specific markers like collagen, fibronectin or smooth muscle actin [4]. The disadvantage of these methods is an inability to follow the tissue reaction in real time *in vivo* [5]. Optical methods such as Late Gadolinium enhanced Cardiac Magnetic Resonance (CMR) are used to detect fibrosis in cardiac tissues even if it is scattered and in low concentration [6]. However, their effectiveness decreases when the patient carries a PCM because it could alter the quality of the image. In addition, due to risk factors, it is contraindicated to apply CMR in patients with PCM, and even if this is done, it is recommended to carry it out weeks after post-implant surgery, which allows a considerable accumulation of fibrous tissue on the electrodes [7]. Chronic monitoring of tissue alteration around implanted electrodes could be a first step to understand this long-term biological process. This

advance could be used to ascertain the treatment effectiveness or to test new biocompatibility strategies of materials.

Electrical Impedance Spectroscopy (EIS) is a well-known technique for characterizing living tissues. Preliminary studies conclude that there is a correlation between the measured resistance and the morphology of the tissue next to the electrode [8]. Amoros-Figueras, *et al.* [9], show that *in situ* impedance measurements in myocardium or epicardium allowed discriminating healthy and infarcted tissue. These results suggest that the tissue remodeling occurring in fibrosis has an EIS signature. Hence, we propose to apply local EIS, taking benefit of the electrodes and the electronic circuitry already existing in PCM, for the continuous and 'low-cost' monitoring of electrode-induced fibrosis. This system should be capable of performing the measurements under the severe condition imposed by the dynamics of the heart, such as the heartbeat movement. Here the impedance must be sensed over the desired frequency range during the short slot time between two consecutive muscle contractions, in order to avoid distorting the measurements, as shown in Figure 1. Therefore, the selected method must meet the following requirements: high measurement speed, flexibility in spectrum manipulation (bandwidth and frequency resolution) and feasibility of the digital implementation.

Based on this strategy we have devised a new EIS measurement approach, fast and flexible, easy to synchronize with the PCM pulses and not affected by the heart dynamics. The innovation is an original application of the Orthogonal Frequency Division Multiplexing (OFDM) technique, well-known and successfully used in the field of digital communication. This technique, here adapted to embedded EIS, exhibits competitive performances, compared to traditional EIS methods, and meet all the previous requirements. This new approach is called hereafter the Orthogonal Multitone Electrical Impedance Spectroscopy -OMEIS-.

This article is structured as following: firstly, the EIS measurement principle and its traditional implementations are presented. Then, the original OMEIS method is described in the second section. Next, we develop the design of an OMEIS prototype, its validation and properties. Subsequently, preliminary experiments are conducted in both *in vitro* and *ex vivo* samples, with living cells and cardiac tissues, respectively. Finally the results obtained in the impedance measurements are discussed.
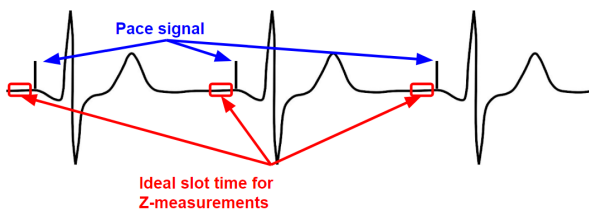

Figure 1. Strategy for measuring cardiac tissue impedance while using the PCM structure. The ECG signal is in black together with the PCM pulse.

2. EIS Overview

The EIS applied to the analysis of a biological material consists of injecting an alternating current or voltage into the tissue under study, and then measuring the resultant (voltage or current, respectively) that appears through the stimulation electrodes. There are several alternating signal generation methods for EIS used for this purpose, with their advantages and disadvantages. These will be discussed next.

2.1. Classic Methods for EIS. The most common signal found in almost all commercial available EIS instruments, due to its implementation simplicity, is the fixed frequency sinusoidal signal. Here the measurements are carried out at a specific frequency, as is the case for these full-custom designs [10, 11], or in a small set of frequencies such as it is found in the commercial instrument xCELLigence [12] which measures the impedance at three discrete frequencies.

When the frequency sweep technique is used, the spectroscopy could be performed within a larger set of determined frequencies. The impedance analysis on a large frequency range provides more insights regarding the tissue features. Gabriel et al. measured the impedance of various organs of the human body in different conditions. The obtained frequency responses are specific signatures for each tissue [13]. This technique presents some limitations in the estimation of time-variable systems or when the impedance estimation of multiple electrodes or samples are needed in a short time frame by the same device. Due to these restrictions, this method does not meet the requirements of the proposed strategy.

2.2. Broadband EIS. Different methods for the generation of broadband signals have been investigated to overcome the limitation of classic approaches. The first approach is dated back to 1975 where pseudo-random binary signals were used for the measurement of an electrode impedance in a wide frequency band [14]. The impedance is estimated by correlating the Sample Under Test (SUT) response with the pseudo-random stimulus signal, which results in the impulse response, following by a Fourier transform. In the case of Maximum Length Sequence (MLS) a more efficient method than correlation has been proposed in [15] based on the Fast Hadamard transform. This kind of signals contains a large range of frequencies and for this reason allows a rapidly impedance spectrum measurement. In addition, pseudo-random signals or MLS are preferred instead of the Dirac pulse, whose high amplitude peak is not desirable for the stimulation of biological samples [16, 17]. The main drawback of this method is the signal amplitude variation at each frequency. The spectrum of a MLS signal is also random and it is possible that the energy at a desired frequency could be too low or equal in amplitude to the noise, which would induce errors in the measurement.

2.3. Multisine Approach. Multisine signals for impedance spectrum measurement of biological samples, reported for instance in [18, 19] and [20], provides also a fast estimation

with the advantage that the Signal to Noise Ratio (SNR) can be improved when using random phases and also that the frequencies can be selected as required, i.e. linear or logarithmic [21]. Such approach is simple however does not scale easily with higher numbers of frequencies. The memory required for the generation of the multisine increases with the number of tones, as it is shown in Table 1 and also found in [22]. Furthermore, the detection and impedance estimation at the receiver side could impede the implementation of this method. It could be verified, in the mentioned references, that the stimulation part could be implemented in digital form by storing in memory the externally created multisine signal. However, the receiving part requires a more complex hardware for the demodulation of the signal, usually implemented by the use of a data acquisition board or system, such as an oscilloscope, and a Personal Computer (PC) for the impedance computation.

2.4. OFDM for our Application. Finally, orthogonal multitone signals also offer a wide spectrum for a rapid impedance estimation in the frequency bandwidth of interest. The generation of this kind of signals could be efficiently implemented by using the OFDM method [23]. This OFDM technique is successfully used in the field of digital communication, however the application for impedance measurement is a novelty and requires of modifications, such as those presented in Section 4. The OFDM method allows to control the spectrum of the multitone signal with great flexibility by defining the values of the OFDM symbols, the use of an appropriate modulation scheme and / or the manipulation of the system parameters, such as the sampling frequency.

Compared to the multisine technique mentioned above, the OFDM method requires less memory for the implementation of the signal generator, as depicted by Table 1. Here the memory required for the multisine and the OFDM approaches for the generation of a broadband signal of length *N.M* is calculated, where *N/2* is the quantity of frequencies of the broadband signal and *M* is the number of multisine periods or OFDM symbols needed to reduce noise by averaging.

As it can be noticed, the pre-calculated (stored in memory) multisine requires *N·M* memory words because it is advisable to apply different random phases on each period of the multisine signal for the improvement of the SNR. However, the normal OFDM approach requires only *2N* memory words because during each cycle only one symbol

TABLE 1: Memory requirement for the multisine and the OFDM approaches for the generation of a *N/2* frequency points broadband signal of length *N·M*.

Approach	Multi-sine worst case	Multi-sine Pre-calculated	OFDM	OFDM Optimized
Memory words	$M \cdot N^2$	$M \cdot N$	$2N$	$\frac{5}{4}N + 1$

of *N* samples is generated and sequentially exit to the Digital to Analog Converter (DAC). This continues, synchronously, until reaching *M* symbols. For these reasons, the OFDM approach is finally the solution that we have retained.

3. OFDM Considerations

The OFDM model used here is composed of *M* blocks of *N* symbols, $X(k,m)$, $k = 0,1,...,N-1$ and $m = 1,2,...,M$, with each symbol modulating one of a set of *N* subcarriers for the generation of the multitone signal. The subcarriers are orthogonal and a cost effective approach is achieved when the Inverse Fast Fourier Transformation (IFFT) algorithm is used, giving the following general equation:

$$x(n,m) = \frac{1}{N}\sum_{k=0}^{N-1} X(k,m) \cdot e^{j\frac{2\pi kn}{N}} \qquad (1)$$

In our application, a low Crest Factor (CF) of the multitone signal is desirable to avoid intermodulation due non-linearities of the analog parts (such as the saturation of the operational amplifiers). We use a simple technique to reduce the CF that consist of generating multiple set of *N* random complex values by controlling the seed and the output delay parameters of a random bit generator, then applying each of them to the OFDM emitter and calculating the CF. The seed and delay yielding the best crest factor is retained. The crest factor is calculated as shown in equation (2):

$$CF = \frac{|x|_{peak}}{x_{rms}} \qquad (2)$$

The output of the IFFT is a sequence of complex values as a function of time. For the sake of simplicity, real-valued signals are assumed hereafter which converts equation (1) into the following equation:

$$\text{Re}\{x(n,m)\} = \frac{1}{N}\sum_{k=0}^{N-1} |X(k,m)| \cdot \cos\left(\frac{2\pi kn}{N} - \theta_X\right) \qquad (3)$$

where $n = 0,...,N-1$ is the discrete time index and $m = 1,...,M$ is the symbol index, being $N \in \mathbb{Z}$ and $M \in \mathbb{Z}$ the IFFT size and the quantity of symbols blocks, respectively and θ_X is the random phase.

One step found in a telecommunication OFDM model is the addition of a Cyclic Prefix (CP) to reduce intersymbol interference caused by a multipath fading channel. This CP consist of taking a copy of N_{cp} elements from the end of the symbol block and concatenating them in front of it. However, EIS measurements do not suffer from Multipath propagation, therefore, instead of a CP, a small Guard Interval (GI) with zeros at the extremes of the frequency band (at 0 and *Fs/2* Hz) will be used to reduce the energy applied on these not useful frequencies.

4. OMEIS System Design, Implementation and Validation

The proposed OMEIS technique is based on the OFDM model explained above, however, some additional modifications are necessary for the implementation of the EIS measuring system as following: the shape and quantity of symbols should be generated taking into consideration the properties that a stimulation signal should have for fast EIS: low voltage, short duration and with a desired spectrum. It should assure that the energy is propagated at the frequency tones under test. Furthermore, a perfect synchronization is required in the implementation, therefore a pilot signal is used. Both additions will be explained in Section 4.1.

In the following, the system will be analyzed into two parts, first the emitting and finally the receiving part.

4.1. The OMEIS Emitter. The emitter function is to generate the stimulation signal with the desired spectrum. The structure of the emitter is shown in Figure 2.a. It consists mainly of symbol generation, synchronization, inverse Fourier transformation and digital to analog conversion stages.

In the symbol generator, the code that gives shape to the multitone signal spectrum is created in a synchronized manner. There are several codes that offer a spectrum with specific differences. For example, a code with constant amplitude generates a spectrum with tones of similar values at the IFFT subcarrier frequencies, that is in $Fp(n)=n·Fs/N$, where Fs is the sampling frequency, N is the size of IFFT and $n = 0, 1, ...,(N/2)-1$. The SUT output to a signal with this spectrum could have an impulse responses that may require rapid sampling to capture the transients. Another

example is a sinusoidal code, with constant frequency Fd, that when applied it is sparsed throughout the whole OFDM bandwidth, locating Fd above and below each subcarrier frequency, resulting in tones with amplitudes at frequencies $Fp(n)-Fd$ and $Fp(n)+Fd$, being this signal a type of multisine. However, although this code does not inject much energy into the IFFT subcarrier frequencies, it could be used in case of nonlinearity analysis. Finally, a random code generates a random spectrum within the frequency bandwidth between 0 and $Fs/2-Fs/N$. However, as mentioned above, there is the possibility of a low amplitude in the frequencies of interest resulting in them being corrupted by noise.

Therefore, one solution is to combine a random code with a constant offset, other than zero, large enough to ensure good amplitude at the carrier frequencies. The latter is provided by a random-bit generator whose output values are mapped with a QPSK modulator and then amplified and shifted with a DC offset. The amplification (G) is selected based on the maximum signal amplitude required and the complex QPSK mapping is used because it introduces a random phase information to the IFFT subcarriers, as shown in eq. (3), that better improves the CF compared to real values mapping such as BPSK [24]. The mathematical backgrounds concerning the performances (BER vs. SNR) of digital modulations show that the OFDM-BPSK and OFDM-QPSK are very similar, but for the CF, QPSK is better [25]. The symbols are generated at a rate of one sample every $1/Fs$ seconds, with a total of N samples per measurement cycle.

Following the symbol generator is the synchronization section. This is a critical step during the calibration stage
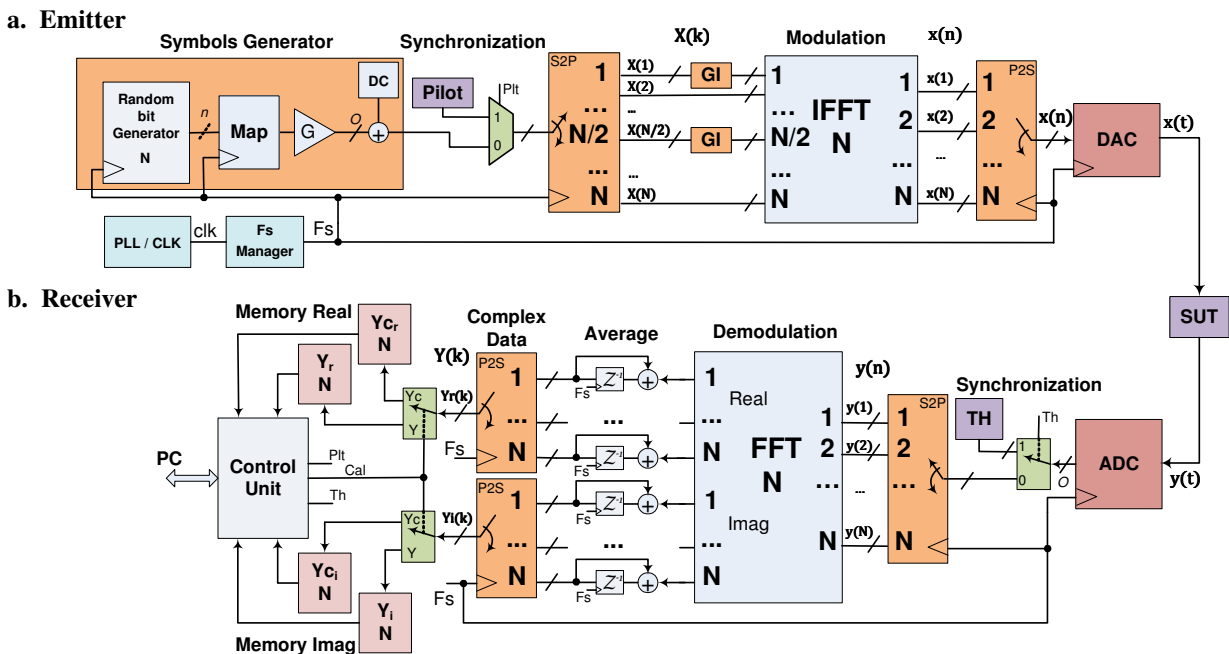

Figure 2.   OMEIS emitter and receiver structures.

because it measures the system delay. This information is used for the correct synchronization between the transmitter and the receiver. Perfect synchronization between both systems is essential to ensure that the selected N input samples of the FFT corresponds to the IFFT transmitted symbol.

The method for synchronization is the following: before calibration, a pilot signal is used which generates voltage peaks at known intervals. The generated peaks can be detected using an appropriate threshold. This method allows the recording of, in one hand, the delay of the transmitter output signal, and on the other, the joint delay of the analog-digital-analog conversions and the AFE stages.

Next is the modulation stage. Here, as explained above, a GI is used before the IFFT. The size of the IFFT (N) gives the quantity of frequency points for the impedance spectrum. The minimum frequency is at Fs/N and the maximum at $Fs/2-Fs/N$ with a frequency separation of Fs/N. Serial to Parallel (S2P) and Parallel to Serial (P2S) blocks are required before and after the IFFT.

Finally, the real output of the IFFT is selected and converted into an analog signal by the DAC.

4.2. The OMEIS Receiver. Once the signal coming from the AFE is encoded by the ADC, the Control Unit multiplexes it, depending on whether it is the pilot signal, which is sent during the synchronization, or the multitone one; sending it to the Threshold detector (TH) or the OFDM demodulation, respectively. At the end of the synchronization, when performing calibration or measurement, the response of the SUT is first demodulated using the FFT, then accumulated with values of previous measurement cycles and finally stored in the corresponding memories: Ycr, Yci in calibration and Yr, Yi in measurement, where r stands for real and i for imaginary.

As it is shown in Figure 2.b, the demodulation produces complex values which are averaged, stored and transmitted independently. The accumulation can increase the number of bits of the samples but reduces the amount of data to be transmitted. The impedance is then estimated with the following equation:

$$Z(\omega) = H_{CAL}(k)\frac{Y(k)}{Y_C(k)} \quad , \qquad (4)$$

where H_{CAL} is the known calibration SUT which may vary in frequency, but nevertheless, it is assumed constant in each cycle of multitone generation; Y is the measurement data and Y_c the calibration data received, $k = 1,2, ..., N$.

At the end of the measurement, when all the computation cycles were performed, the resulting calibration and measurement data are sent to a PC for the final treatment and display.

4.3. The OMEIS Implementation. The modified OFDM structure, detailed in the preceding sections, is suitable for embedded systems. The implementation takes advantage of the computing power and the parallel features of FPGAs,

performing both emitter and receiver in a Cyclone IV FPGA device programmed in VHDL language.

Figure 3, shows the OMEIS system implementation. The emitter part of the OMEIS system is implemented by using the IFFT and the PLL Clock generator Megacores IP. The remaining block, for instance the Cell Automata (CA), the Fs Manager, the Pilot, and the QPSK blocks, were coded in VHDL.

The values of the emitter's parameters, such as IFFT size or sampling frequency can be adjusted as required. The default value used for the IFFT size is 1024. The Fs Manager allows to change the sampling frequency Fs of the system to 1 MHz, 500 kHz and 250 kHz.

The Symbol Generator is the combination of the CA and the QPSK blocks. First the CA uses a Cellular Automata algorithm for the creation of two (2) random bits that are next mapped in the following way: for bits *"11"* the QPSK output is $(G+jG)+DC$, *"10"* gives $(G-jG)+DC$, a *"01"* is $(-G+jG)+DC$ and finally *"00"* results in $(-G-jG)+DC$, where G is 1023 and DC equal to 80 in our implementation, both values were selected taking into consideration the output voltage amplitude and frequency spectrum shape.

A synchronous state machine, which operates as a Control Unit (CU), manages the overall behavior of the system. Both, the CU and the DAC/ADC manager are coded in VHDL as well.

An Analog custom board has been developed in order to perform EIS in biological samples. It has a parallel input 12
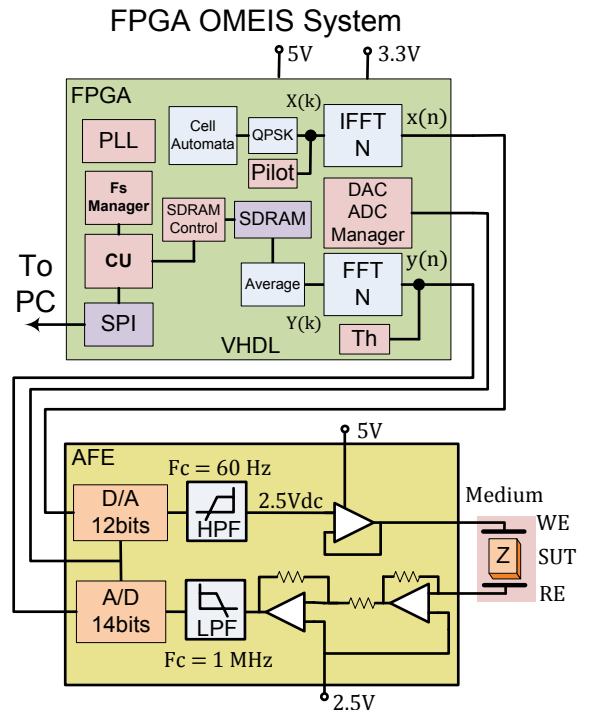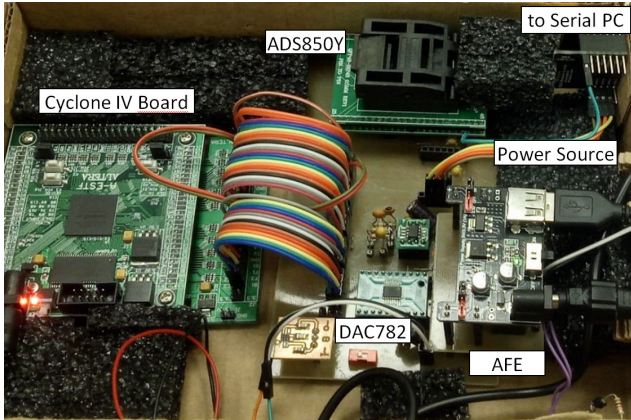

Figure 3. The OMEIS System schematic.

Figure 4. The OMEIS System board.

Figure 5. Hardware resource utilization of the OMEIS emitter implemented in a Cyclone IV FPGA.

bits DAC converter (DAC7821), a parallel output 14 bits ADC (ADS850Y) and an Analog Front End (AFE) board, as depicted in Figure 4. This AFE board has maximum stimulation voltage amplitude of 200 mV, low output impedance and a very low voltage offset between Working Electrode (WE) and Counter Electrode (CE), which are required for biological measurements. Additionally, the AFE filters non desired DC and 50/60 Hz components from the multitone signal. The stimulation signal is voltage and the resulted current is capture and converted into voltage via a Transimpedance Amplifier (TIA) in which the values of a feedback resistor is set during calibration.

At the receiver side, the demodulator is implemented using the FFT Megacores of Altera. The size of the FFT is the same as that of the IFFT. Both the calibration and the SUT data, coming from the average block are stored in a 256 Mb SDRAM (W9825G6EH). Then they are sent via SPI to a PC. The PC runs a Human-Machine Interface (HMI), coded in Matlab, for the control of the system as well as for the analysis of the data received running equation (4) for the final impedance estimation. The OFDM TH block, coded in VHDL, employs a threshold algorithm to detect the pilot signals and compute the transmitted signal output delay and the system response delay to send them to the CU.

Figure 5 shows the cost in hardware resources of the OMEIS emitter as a function of the IFFT size N. The values of resources for $N = 1024$ are depicted on the plots. The number of multipliers is 24 for all N. Notices that N is double the quantity of frequencies of the multitone signal.

4.4. The Orthogonal Multitone Spectrum. The orthogonal multitone signal was analyzed by using the OMEIS implementation configured with a sampling frequency of $Fs = 1$ MHz, 32 symbols and an IFFT size of $N = 1024$ giving a multitone subcarrier frequency separation of 976.5 kHz. Also, a gu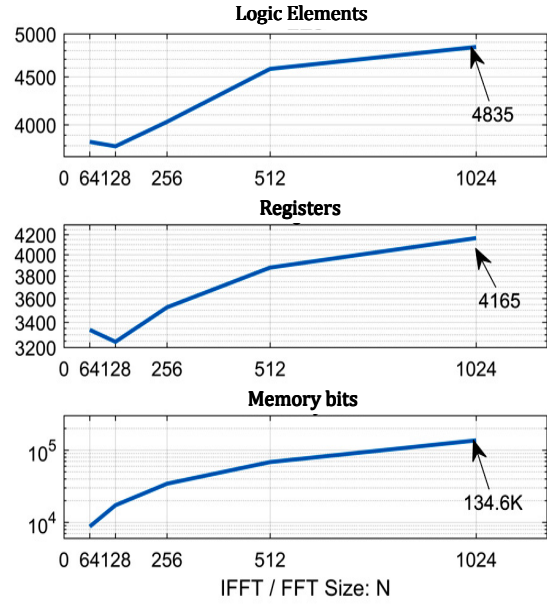ard interval of 10 frequencies points at the end of the spectrum is applied giving a maximum frequency of 488.28 kHz. Furthermore, to test the frequency selection capabilities of the system, the subcarriers were also eliminated in the range from $n = 100$ to $n = 150$, which corresponds to a bandwidth of 97.65 kHz to 146.48 kHz ($F(n)=n \cdot Fs/N$). A digital oscilloscope (Tektronic DPO500B), with FFT function capabilities, is used to measure the spectrum of the signal during this test.

Figure 6 shows the spectrum of the stimulation multitone voltage signal (above) and the voltage signal spectrum of a resistance $Rn = 671.8$ Ω (below), that is connected in series with the test impedance ($Rs + Rp \parallel C, Rs = 265.4$ Ω, $Rp = 4.62$ kΩ, $C = 1.1$ nF). The second signal was intentionally displaced 20 dB below, in the Figure, for better visibility.

As shown in Figure 6 above, the spectrum of the multitone signal has a flat shape between 0 Hz to 488.281 kHz, with the exception of the removed bandwidth measured between 97.65 kHz and 146.5 kHz.

When the voltage spectrum of the resistance Rn is measured (Figure 6, below), the amplitude of the spectrum changes as expected: At the frequency of 488.28 kHz, where the test impedance "Z" is about 410 Ω, the amplitude is about -23.57 dB, that is -4.2 dB less than the multitone signal amplitude of -19.37 dB. This very closely corresponds to the theoretical difference of $20\log(671.8/(410+671.8)) = -4.13$ dB. At low frequency (19.5 KHz, Z = 4.2 kΩ) the delta marker shows -16.2 dB that also is very similar to the theoretical $20\log(671.8/(4.2k+671.8)) = -17$ dB.
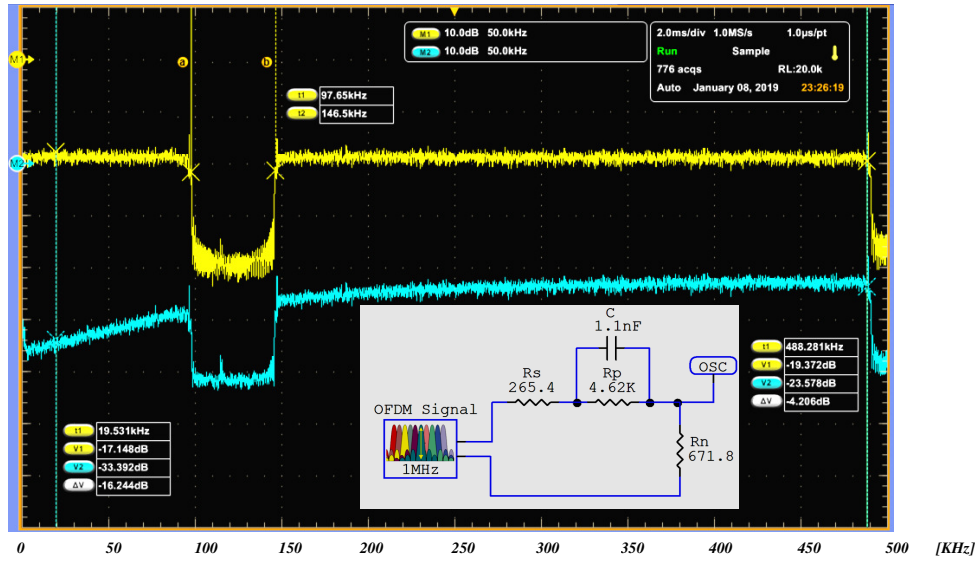
Figure 6. Spectrum of a resistance *Rn* voltage signal (below) form a voltage divider circuit between *Rn* and the test impedance powered by the multitone signal (spectrum above). The values of the test impedance is shown. The markers (ΔV) show the amplitude difference, in dB, between both spectrum at the frequency of 19.53 kHz and 488.28 kHz. The second signal was intentionally shifted 20 dB down for better visibility.

4.5. The OMEIS System Performance. For the validation of the OMEIS system, the size of the IFFT and the FFT is 1024 and the *Fs* = 1 MHz. Therefore, there are 511 available frequency points for the impedance estimation with a spectrum resolution and first frequency point of 976.5 Hz (DC frequency is not calculated). The stimulation time depends on Fs, the size of the IFFT / FFT (*N* = 1024) and the symbols quantity (*M* = 32 in this case), resulting in 32.76 ms. *M* also corresponds to the number of measurement cycles used for averaging. This test was performed by using a test circuit (Rs=750 Ω , Rp=30 kΩ, Cp=2 nF), as shown in Figure 7. The result shows a good accuracy in the impedance estimation with a 1.39% mean error.
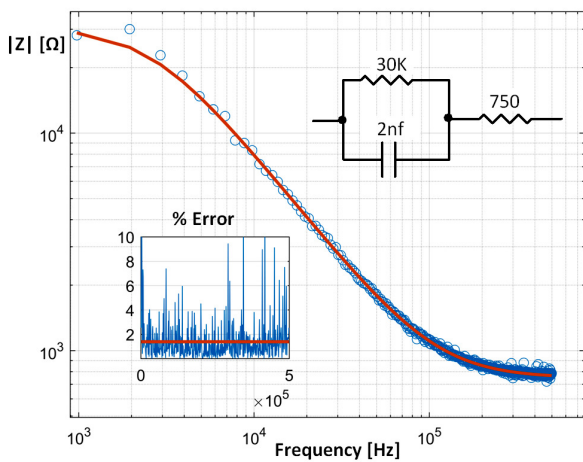

Figure 7. Impedance comparison between model (red) and the estimation from the OMEIS system (blue).

5. Experiments

After having characterized the performances of our system in terms of hardware resources, signal spectrum and impedance estimation, we proceed to the presentation of preliminary results of *in vitro* and *ex vivo* experiments performed under conditions related to fibrosis. First, we describe experiments with cell cultures, in which the correlation between the impedance and the cell population is observed. OMEIS's spectrum management and frequency resolution flexibility is tested as well. Finally, *ex vivo* impedance measurements conducted on inhibited and perfused porcine heart tissue are described, using commercial human PCM probes, for a more realistic condition.

5.1. In Vitro Measurements. These tests focus on the flexibility of the OMEIS system and the estimation of errors during biological sample measurements.

5.1.1. *Materials.* A commercially available cultureware of Applied Biophysic Inc. [26], shown in Figure 8, is used during the experimentation. The cultureware consists of an array of 8 wells with 10 electrically interconnected circular gold electrodes (250μm diameter) on each well and one central larger electrode common to all wells. The electrodes are delineated with an insulating film. The cultureware offers a two electrodes setup for EIS measurement: the Working Electrode (WE) and the Counter Electrode together with the Reference Electrode (CE and RE).

The OMEIS system was calibrated with a IFFT/FFT size *N=1024*, a symbols quantity of 32 and with 3 values for *Fs* of 1 MHz, 500 kHz and 250 kHz. There is a GI at DC and at the first and the last frequencies (*Fs/N* and *Fs/2*). The minimum frequency (Fm), the frequency separation (ΔF)

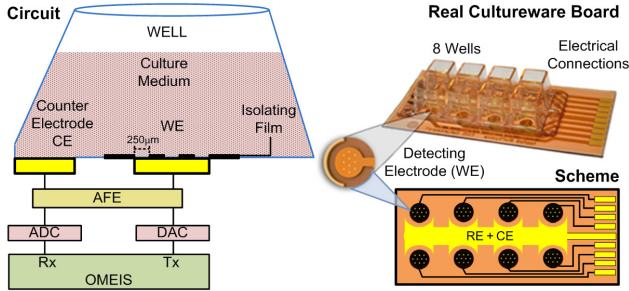| Fs [MHz]	Fm [Hz]	ΔF [Hz]	Ts [ms]
1	1952	976	65.5
0.5	976	488	131
0.25	488	244	262

Figure 8. The circuit of the electric cell-substrate impedance sensing (ECIS) protocol and the OMEIS system. Also, the picture and the scheme of the ECIS cultureware board (8W10E) with eight mini wells (∼0.6 mL) are depicted.

and the stimulation time (Ts) for each configuration are shown in Table 2.

5.1.2. *Protocol.* The in vitro experimentations are performed on immortalized mouse myoblast cell line (C2C12 cells.) Under appropriate conditions, they are cells that produce proteins related to fibrosis [27]. The protocol for in vitro cell-substrate EIS measurements is the following: at the beginning of the experiment, one well of the cultureware was filled with 7,000 C2C12 myoblast plus a 600 μL of Dulbecco's Modified Eagle's Medium (DMEM) containing 10% Fetal Bovine Serum (FBS), sodium bicarbonate (3.7 g/L) and 1% antibiotics. Other well was filled with only 600 μL of medium and is used as control well. Cells were cultured in an incubator at 37°C and 5% CO_2 and the medium was changed every 48 hours. Five measurements were taken during the 95 hours of incubation, enough time for a development of a large cell population on the electrode. Visual inspections were performed with a standard inverted microscope.

5.1.3. *Results.* Figure 9.a shows the impedance spectrum at five measurement times when *Fs* = 1 MHz: times 0h, 23h, 47h, 71h and 95h (h stand for hours after the beginning of the experimentation). In the frequency domain the spectrum shows a negative constant slope, whose magnitude differs depending on the measurement time, from the first *frequency up to the 20 kHz, when it begins to decrease.*

The evolution of the impedance in time could be better evaluated by using the Figure 9.b, where the normalized impedance is depicted, taking time 0h as the reference [Measured impedance at point k divided by the Impedance of time 0h at the same point k]. As shown, the impedance module increases from 1.5 at time 23h and frequency 55 kHz to almost 3.5, at time 95h and frequency 95 kHz, in
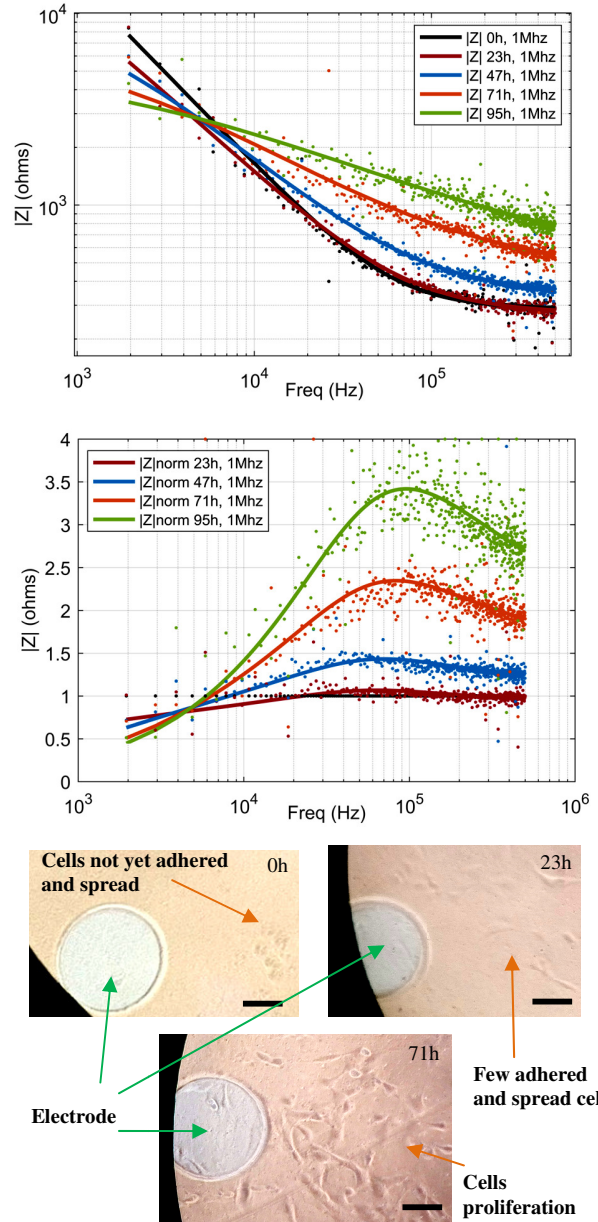

Figure 9. Impedance spectrum performed on C2C12 cells cultured *in vitro*. Five measures were taken at 0, 23, 47, 71 and 95 hours. a) Impedance Module. b) Normalized impedance. c) Microscopy photos at 0h, 23h and 71h. The scale bar represents 100 μm.

correspondence with the increase of the cell population in the electrode. This is validated using microscopy photos to visually correlate the state of the culture with the measurements, Figure 9.c.

For the study of the flexibility of the system, the impedances at 3 sampling frequencies are evaluated together. Here we are using the sampling frequencies of 1 MHz, 500 kHz and 250 kHz that give the frequency resolution of 976 Hz, 488 Hz and 244 Hz, respectively. As expected, the impedance at the same measurement time but

at different sampling frequencies overlaps, as shown in the Figure 10. This flexibility allows the addition of more frequency points for a better evaluation of the regions of interest. It should be noted that the sampling frequency can be changed by software, either manually or automatically without the need to reconfigure the system.

The results obtained in these experiments show that the frequency band from 30 kHz to 200 kHz is optimal for the observation of the impedance signature corresponding to the growth of the cell population.
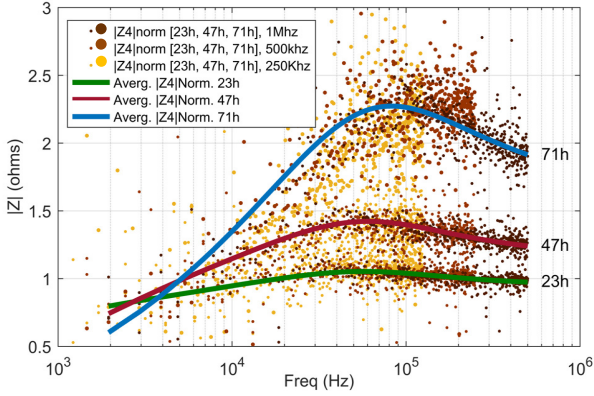

Figure 10. Normalized impedance of the C2C12 cells at times 23h, 47h and 71h (h = cell culture time in hours), when using 3 different sampling frequencies.

5.1.4. *In vitro Experiments Data Modeling.* Data presented in Figure 9.a were used in a impedance model identification algorithm. Due to the bandwidth of the measurements (2 kHz to 500 kHz) and the limited double layer capacitance associated with the micro-electrodes used, the observable behavior is associated with the cell membrane and the intra and extracellular medium [28]. The electrode impedance is fitted in our case with the following equation:

$$Z_{elec}(f) = R \frac{1+\left(j\frac{f}{f_u}\right)^{\gamma}}{\left(j\frac{f}{f_u}\right)^{\gamma}} \ , \qquad (4)$$

where R is the resistance at high frequency, γ is the fractional order of the constant phase element and f_u the transition frequency.

Data were fit by minimizing the residual function of the distance between the measurement and the modeled data using a Powell method [29]. Results are given in the following table:

TABLE 3: Data fit parameters results

t (hours)	R (Ω)	γ	f_u (kHz)	NRMSE
0	281	0.93	59.2	0.0138
23	265	0.87	69.2	0.0153
47	321	0.80	79.3	0.0098
71	358	0.54	201.0	0.0386
95	495	0.45	215.0	0.0314

In high frequency, the resistance R shows a slight increase over time. Nevertheless, there is a clear evolution of the Constant Phase Element (CPE) order from values near 1, corresponding to a pure integrator of capacitor, to values around 0.5, corresponding to a Warburg CPE. As the measurements were performed over a single well, no conclusion on the correlation between the model parameters and the biological evolution of the cells can be drawn. However, the measurement method clearly enables to observe changes in the electrical impedance over time for the targeted application. Moreover, the measurement data can fit standard electrode impedance model using conventional optimization algorithms.

5.2. Ex Vivo Measurements. The OMEIS flexibility and reliability during impedance measurement have been proven in Section 5.1. The objective now is the evaluation of OMEIS ability for *in vivo* conditions. The following experiments are conducted on the cardiac tissues, *ex vivo*, freshly explanted, using a commercial pacemaker electrode. Two types of characterization are performed on ventricles of a swine heart: first on a tissue immersed in a cardioplegic solution that inhibits the cardiac contractions and second on perfused tissue that mimic in vivo conditions.

5.2.1. Materials. The measurements were performed with the OMEIS system and the commercial lab instrument Solartron 1260 (Ametek, USA), which is an impedance spectrometer commonly used for bioimpedance measurements. A human PCM cardiac lead, Sprint Quattro Secure 6947M (Medtronic, USA) is used as sensing electrode. This lead has both pacing and defibrillation electrodes, but for this experimentation only the pacing termination was used.

5.2.2. Animal Model. This study was carried out in accordance with the recommendations of the Directive 2010/63/EU of the European Parliament on the protection of animals used for scientific purposes and approved by the local ethical committee of Bordeaux CEEA50. The heart was obtained from a young swine (Large White, 40±5 kg). The swine was pre-medicated with ketamine (20 mg/kg) and acepromazine (Calmivet, 1mL/50kg). Anesthesia was induced with intravenous injection of sodium pentobarbital (10 mg/kg) and maintained under isofluorane, 2%, in 100% O_2. The swine was euthanized by sodium pentobarbital (40 mL, from 50 mg/mL of stock) and the heart rapidly excised, cannulated by the aorta, and rinsed with cold cardioplegic solution, containing (mM): NaCl, 110; $CaCl_2$, 1.2; KCl, 16; $MgCl_2$, 16; $NaHCO_3$, 10; and glucose, 9.01 at 4°C.

5.2.3. Protocol in Cardioplegia. The right ventricle (RV) wall was dissected and placed in the cardioplegic solution (in mM: 110 NaCl, 1,2 $CaCl_2$, 16 KCl, 16 $MgCl_2$, 10 $NaHCO_3$, 10 glucose) and then chilled with ice during the measurements.

The OMEIS system was configured with an IFFT/FFT of size $N = 1024$, 32 symbols and a $Fs = 1$ MHz. For the Solartron 1260, the measurements were done at a 100 mV peak voltage level (similar to the OMEIS system), with a logarithmic frequency sweep from 1 MHz to 0.1 Hz, with 10 points per decade. For OMEIS, each measure was carried out only once, for the Solartron they were repeated five times and the mean of these five measurements is calculated.

The *ex vivo* measurements were performed in two different endocardial regions of the ventricle: the healthy lateral wall and a more 'collagen' rich region near the basal area and auriculo-ventricular ring. From now on, the normal endocardium tissue will be termed 'Muscle' and will be compared to the 'Collagen' region. The first region is where the lead is placed in Figure 11, and the second one is the region just above the tricuspid valve (white tissue in Figure 11.)
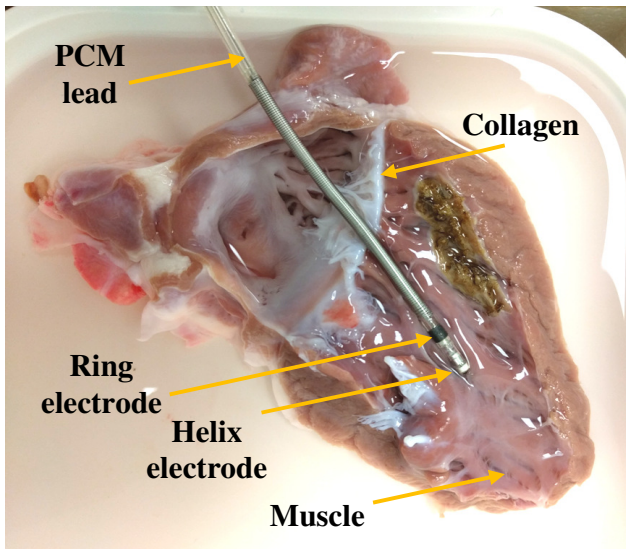

Figure 11. *Ex vivo* experimentation on a swine heart. Right Ventricle (RV) placed in cardioplegic solution. Pacemaker lead in the endocardial 'Muscle' region.

5.2.4. Protocol for Perfused Tissue. Figure 14 shows the Langendorff system used for the perfusion protocol in this section: The left ventricle (LV) was dissected and cannulated by the left anterior descending artery. Then, the LV was mounted on to a frame where it is submerged and perfused (20 mL/min) with a warm (37°C) saline solution containing (mM): NaCl, 130; NaHCO$_3$, 24; NH$_2$PO$_4$, 1.2; MgCl$_2$, 1; glucose, 5.6; KCl, 4; CaCl$_2$, 1.8; gassed with 95% O$_2$/5% CO$_2$ at 37°C (pH 7.4). A volume-conducted ECG was measured in the bath to monitor the electrical activity of the tissue preparation.

The ventricle was stimulated from the epicardium at 1 Hz using bipolar tungsten electrodes coupled to a pulse generator and constant current stimulator (DG2A, DS3, Digitimer, UK). The stimulation currents were applied at twice the excitation threshold for a duration of 2ms.

5.2.5. Results of Inhibited Cardiac Tissue Experiments. In the following, measurements of impedance spectrum were first performed with Solartron then with OMEIS.

Figure 12 shows the impedance spectrum measured in the different heart regions as well in the Cardioplegic solution (CPG) by both instruments. It can be noticed that the 'Muscle' has the greatest magnitude of impedance, followed by the 'collagen' region and lastly the CPG solution that has a much lower impedance of around 190 Ω.

The values of the OMEIS system were noisy due to the fact that a reduced number of symbols ($M = 32$) was used in order to increase measurement speed. However, the averaged version follows very closely the values of the reference instrument with a mean error of about 8% and a standard deviation of 5.8%. This allow a differentiation between the impedance of the tissues.
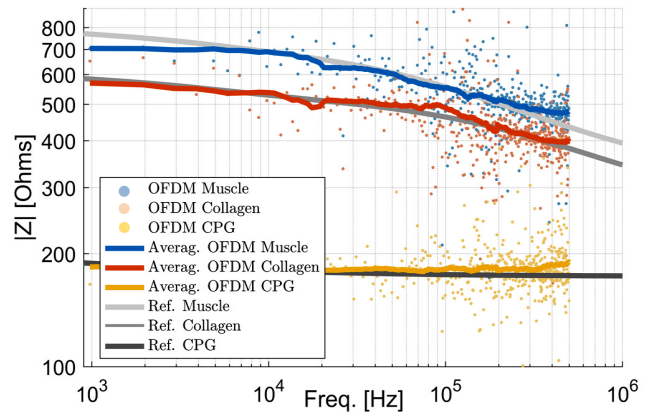

Figure 12. Magnitude of impedance measurement for 3 conditions: 'Muscle' stands for normal endocardial region, 'Collagen' for collagen region and 'CPG' for Cardioplegia. OFDM is performed at Fs = 1MHz. Colored curves represent OMEIS measurements, grey curves represent Solartron measurements.

5.2.6. Results of Cardiac Tissue Perfusion Experiments. During the experimentation with the heart in the perfusion state, the OMEIS system delivered valid results, however, the Solartron yielded meaningless values. We attribute this anomaly, in the reference instrument, to the electro-physiological and mechanical activities of the heart. These behave like a time invariant system that could not be sensed by an instrument that uses the frequency sweep EIS method.

Figure 13 shows the impedance values received from the OMEIS in the perfusion condition, for the 'Muscle' and 'Collagen' regions. It can be noticed that again the 'Muscle' tissue has a greater impedance than the 'Collagen' although, both lower than the values obtained in the first experience described above. Experimental conditions differ indeed largely, especially in temperature, and also in the fact that both the heart and the electrode were here completely submerged in the saline solution.

Furthermore, the Sprint Quattro Secure 6947M pacing lead has two poles, the proximal electrode (helix electrode) is inserted in the tissue and the distal electrode (larger ring)

is used as the returning current path. In the first experiment, cardiac tissue is immobilized and the ring electrode relies simply on the tissue, as can be seen in Figure 11. In the second experiment, the perfused cardiac tissue is immersed and exhibits contractions; the ring electrode is certainly no more in contact with the tissue but moves in the liquid. However, with the impedance measurement the differentiation between both tissues is possible, even with the dynamic of the heart imposed by the perfusion system.
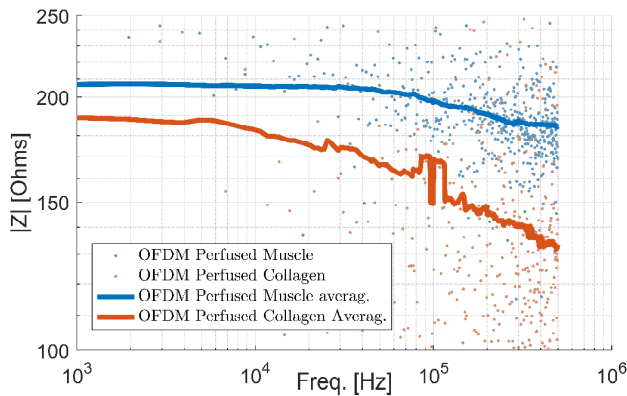

Figure 13. Magnitude of impedance of the Muscle and the Collagen regions with the heart in perfusion, measured by the OMEIS system at Fs = 1 MHz.

6. Conclusion and Perspectives

In this article we propose a novel strategy for the chronic detection of fibrosis induced by the electrodes of cardiac implants. This strategy consists of the application of Electrical Impedance Spectroscopy (EIS) as a technique for sensing fibrosis at short intervals between the peacemaker pulses and the heartbeat. Given the speed and flexibility requirements in the measurement, in addition to the constraint of low hardware cost that this strategy imposes, we have devised, as a innovative solution, the use of orthogonal multitone signals combined with the OFDM implementation method, resulting in the Orthogonal Multitone EIS -OMEIS- approach.

This proposed OMEIS system is prototyped on a FPGA based platform that provides an adjustable sampling frequency and IFFT/FFT size, with a default value of 1 MHz and 1024, respectively. With the default setup, the system offers a maximum OFDM multitone signal bandwidth of 499 MHz with 511 subcarriers separated 976.5 Hz. This system is validated through experiments with electrical circuits resulting in an impedance spectrum with an average error of 1.39% when using 511 frequencies and an amount of 32 OFDM symbols. In addition, the measurement capacity of biological samples and the flexibility of the OMEIS system were studied by mean of measurements of living cell in *in vitro* cultures. It showed a good correlation between the magnitude of the impedance and the cell population at sampling frequencies of 1 MHz, 500 kHz and 250 kHz, when measuring in different times C2C12 cells cultivated during a period of 95 hours. The adjustment of the sampling frequency can be done manually or automatically, on the flight, without the need to reconfigure the system.

Finally, the strategy mentioned at the beginning has been validated by *ex vivo* measurements of cardiac tissue in inhibited and in perfusion states. In the first case, the OMEIS system showed impedance spectrum that, once averaged, were similar to that of the reference instrument, with an 8% average error and 5% standard deviation. In the second case, given the dynamics of the perfusion system, only the OMEIS performed measurements as expected. The
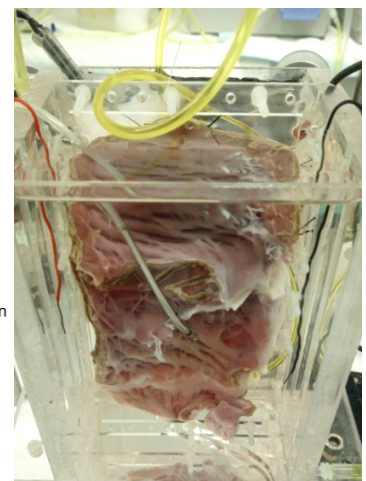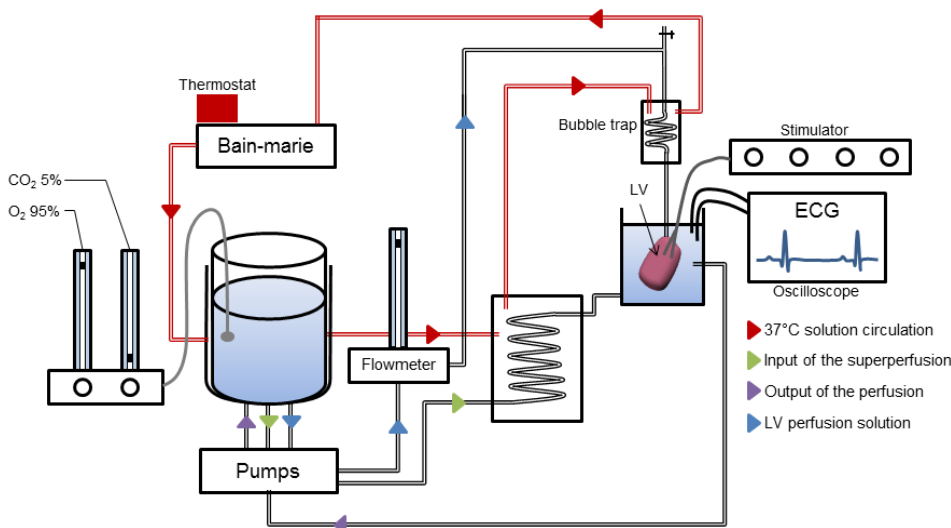

Figure 14. Langendorff system maintaining the ventricle in the in vivo conditions. A picture of the heart inside the perfusion chamber is shown at right.

acquired values from OMEIS allow us to distinguish between 'Muscular' tissue from the 'Collagen' tissue.

Since the cells used for the *in vitro* experimentation produce collagen in the extracellular matrix, and due the fact that fibrosis tissue is composed mainly by collagen (with few cells), we have performed both experimentation (*in vitro* and *ex vivo*) in order to study the OMEIS system in both scenarios. As shown in the *in vitro* results, when the cells reproduce the impedance also increases, therefore as it is shown in the *ex vivo* experimentation, the "collagen" region has a lower impedance than that of the "muscle" (full of cells) tissue.

The performance in the measurement speed is inside the requirements, giving 510 frequency points in a stimulation time of about 64 ms with the OMEIS parameters: $N = 1024$, $M = 32$ and $Fs = 1$ MHz.

The tradeoff between the noise reduction and the symbol quantity is a critical step in the calibration of the system. We were using 32 symbols that showed good results during electrical circuits and *in vitro* experimentations, but that was in the limit for the *ex vivo* experimentation. The increase of the symbols quantity should solve the problem with the cost of reducing the measurement speed, however this solution should be carefully analyzed in order to remain in the time frame required for the proposed strategy. Another solution could be the use of another OFDM code, that with the appropriated modulation scheme, could improve better the CF. These are topics for future research in our group to further improve the OMEIS system since it is the tool that will allow us to establish an electrical signature of a fibrotic tissue.

Conflict of Interest Statement

The authors declares that there is no conflict of interest regarding the publication of this paper.

References

[1] B. Rolfe et al., The Fibrotic Response to Implanted Biomaterials: Implications for Tissue Engineering, Chapter 3 in Regenerative Medicine and Tissue Engineering - Cells and Biomaterials, Edit. D. Eberli, Publish. InTech, 2011.

[2] W. M. Grill and J. Thomas Mortimer, "Electrical properties of implant encapsulation tissue," Ann. Biomed. Eng., vol. 22, no. 1, pp. 23–33, 1994.

[3] H. Mase, K. Tamura, A. Hiromoto, M. Hotta, S. Hotomi, M. Togashi, Y. Fukuda, T. Yajima, T. Nitta, S. Tanaka, and Y. Sugisaki, "Histopathological study of tissue reaction to pacemaker electrodes implanted in the endocardium.," J Nippon Med Sch, vol. 72, no. 1, pp. 52–59, 2005.

[4] S. De Jong, T. A. B. Van Veen, J. M. T. De Bakker, M. A. Vos, and H. V. M. Van Rijen, "Biomarkers of myocardial fibrosis," J. Cardiovasc. Pharmacol., vol. 57, no. 5, pp. 522–535, 2011.

[5] G. C. McConnell, R J Butera and R V Bellamkonda, Bioimpedance modeling to monitor astrocytic response to chronically implanted electrodes, J. Neural Eng. 6, 2009.

[6] N. Akoum, C. McGann, G. Vergara, T. Badger, R. Ranjan, C. Mahnkopf, E. Kholmovski, R. MacLeod, and N. Marrouche, "Atrial fibrosis quantified using Late Gadolinium Enhancement MRI is associated with sinus node dysfunction requiring pacemaker implant," J. Cardiovasc. Electrophysiol., vol. 23, no. 1, pp. 44–50, 2012.

[7] Yokoyama K, Kariyasu T, Kuhara S, Imai M, Ishimura R, et al., "Influence of MRI-Conditional Cardiac Pacemakers on Quality and Interpretability of Images Acquired in 1.5-T Cardiac MRI," Int. J. Clin. Cardiol., 2:030, 2015.

[8] W. M. Grill and J. Thomas Mortimer, "Electrical properties of implant encapsulation tissue," Ann. Biomed. Eng., vol. 22, no. 1, pp. 23–33, 1994.

[9] G. Amorós-figueras, E. Jorge, T. García-sánchez, and R. Bragós, "Recognition of Fibrotic Infarct Density by the Pattern of Local Systolic-Diastolic Myocardial Electrical Impedance," vol. 7, no. August, 2016.

[10] R. Gonzalez-Landaeta, O. Casas and R. Pallas-Areny, "Heart Rate Detection From Plantar Bioimpedance Measurements," in IEEE Transactions on Biomedical Engineering, vol. 55, no. 3, pp. 1163-1167, March 2008.

[11] K. Kim et al., "A 24 μW 38.51 mΩrms resolution bio-impedance sensor with dual path instrumentation amplifier," ESSCIRC 2017 - 43rd IEEE European Solid State Circuits Conference, Leuven, 2017, pp. 223-226.

[12] Calculation principles of RTCA Software, Technical Note No. 2, xCELLigence System, Jan. 2010.

[13] S. Gabriel, R. Lau, and C. Gabriel, "The dielectric properties of biological tissues : II. Measurements in the frequency range 10 Hz to 20 GHz," Phys. Med. Biol., vol. 41, pp. 2251–2269, 1996.

[14] G. Blanc, I. Epelboin, C. Gabrielli, and M. Keddam, "Measurement of the elecrode impedance in a wide frequency range using pseudo-random noise," Electrochim. Acta, vol. 20, no. 8, pp. 599–601, 1975.

[15] M. Cohn and A. Lempel, "On Fast M-Sequence Transforms," IEEE Trans. Inf. Theory, vol. 23, no. 1, pp. 135–137, 1977.

[16] I. Schneider, "Broadband signals for electrical impedance measurements of long bone fractures," 18th Annu. Int. Conf. IEEE Eng. Med. Biol. Soc., pp. 1934–1935, 1996.

[17] T. Sun, C. van Berkel, N. G. Green, and H. Morgan, "Digital signal processing methods for impedance microfluidic cytometry," Microfluid. Nanofluidics, vol. 6, no. 2, pp. 179–187, 2009.

[18] R. Bragos, R. Blanco-Enrich, O. Casas, and J. Rosell, "Characterisation of dynamic biologic systems using multisine based impedance spectroscopy," IMTC 2001. Proc. 18th IEEE Instrum. Meas. Technol. Conf. Rediscovering Meas. Age Informatics (Cat. No.01CH 37188), vol. 1, no. 1, pp. 44–47, 2001.

[19] T. Breugelmans, E. Tourwé, J. B. Jorcin, A. Alvarez-Pampliega, B. Geboes, H. Terryn, and A. Hubin, "Odd random phase multisine EIS for organic coating analysis," Prog. Org. Coatings, vol. 69, no. 2, pp. 215–218, 2010.

[20] B. Sanchez, G. Vandersteen, I. Martin, D. Castillo, A. Torrego, P. J. Riu, J. Schoukens, and R. Bragos, "In vivo electrical bioimpedance characterization of human lung tissue during the bronchoscopy procedure. A feasibility study," Med. Eng. Phys., vol. 35, no. 7, pp. 949–957, 2013.

[21] B. Sanchez and R. Bragos, "Fast Electrical Impedance Spectroscopy for Moving Tissue Characterization Using Bilateral QuasiLogarithmic Multisine Bursts Signals," IFMBE Proc., vol. 22, pp. 1084–1087, 2008.

[22] E. De Roux, M. Terosiet, F. Kolbl, M. Boissière, E; Pauthe, et al., "Toward an Embedded OFDM-based System for Living Cells Study by Electrochemical Impedance Spectroscopy," *Proceedings of IEEE HealthCom Conference*, Sep 2018, Ostrava, Czech Republic.

[23] S. B. Weinstein and M. Ebert, Paul. "Data Transmission by Frequency-Division Multiplexing Using the Discrete Fourier Transform," *Communication Technology*, IEEE Transactions no. 19, 628 - 634, 1971, DOI: 10.1109/TCOM.1971.1090705.

[24] S. Boyd, "Multitone Signals with Low Crest Factor," *IEEE Trans. Circuits Syst.*, vol. CAS-33(10), pp. 1017–1022, 1986.

[25] NeetuSood, Ajay K Sharma, MoinUddin, "BER Performance of OFDM-BPSK and -QPSK over Nakagami-m Fading Channels," In Proceeding of IEEE-IACC'2010, Patiala, India, Feb. 2010.

[26] Applied BioPhysics. "ECIS: Electric Cell-Substrate Impedance Sensing," Internet: http://www.biophysics.com/Product

Sheets/Applied BioPhysics Technology and Product Guide.pdf, pp. 35, 2018.

[27] Li Y, Foster W, Deasy BM, et al. "Transforming Growth Factor-β1 Induces the Differentiation of Myogenic Cells into Fibrotic Cells in Injured Skeletal Muscle : A Key Event in Muscle Fibrogenesis". The American Journal of Pathology. 2004;164(3):1007-1019.

[28] S. Grimnes, O. Rikshospitalet and N. Schwan, "Interface phenomena and dielectric properties of biological tissue,"' Encyclopedia of surface and colloid science, 2002, vol. 20, p. 2643-2653.

[29] M.J.D. Powell, "An efficient method for finding the minimum of a function of several variables without calculating derivatives," The computer journal, 1964, vol. 7, no 2, p. 155-162.